Ciência Rural, Santa Maria, v.53:10, e20210914, 2023
http://doi.org/10.1590/0103-8478cr20210914
ISSNe 1678-4596
SOIL SCIENCE

Chromium adsorption studies using brewer's spent grain biochar: kinetics, isotherm and thermodynamics

Rodrigo Geremias[1] Catiane Pelissari[1*] Nelson Libardi[2] Danielle Carpiné[3] Rosemary Hoffmann Ribani[3]

[1]Universidade do Oeste de Santa Catarina (UNOESC), 89566-252, Videira, SC, Brasil. E-mail: catiane.pelissari@unoesc.edu.br. *Corresponding author.
[2]Universidade Federal de Santa Catarina (UFSC), Florianópolis, SC, Brasil.
[3]Universidade Federal do Paraná (UFPR), Curitiba, PR, Brasil.

ABSTRACT: Brewer's spent grain (BSG) is a residue from brewery production, that can be reused as adsorbent of heavy metals like Chromium (Cr). In this study, BSG was used as a biochar for Cr adsorption in batch adsorption experiments. The biochar pyrolysis temperature (500, 600 and 700ºC), pyrolysis time (30, 105 and 180 minutes) and zinc chloride concentration (5, 12.5 and 20%) were evaluated and optimized from a fractional factorial design. An equilibrium adsorption capacity of 78.13 mg.g^{-1} and a yield of 26.42% were achieved using 700ºC, 30 min, 12.5%. This biochar was applied to the adsorption of Cr in aqueous solution, under different stirring speeds (100, 150 and 200 rpm). The higher agitation speed reduced the adsorption capacity of the coal from 90 to 72 mg.L^{-1}. In addition, the Cr adsorption equilibrium was reached before 100 min. The pseudo-first order model best described the Cr adsorption kinetics. The Redlich-Peterson isothermal model best fitted the experimental data, with the parameter g (close to 1) suggesting Langmuir's assumptions as the most appropriate to describe the adsorption of Cr on the optimized activated carbon.
Key words: biosorption, chromium removal, activated carbon, brewer's waste.

Estudo da adsorção de cromo usando biochar proveniente de bagaço de malte: cinética e termodinâmica

RESUMO: O bagaço de malte (BM) é um resíduo da produção cervejeira, que pode ser reaproveitado como adsorvente de metais pesados como o Cromo (Cr). Neste estudo, BM foi usado como um biochar para adsorção de Cr em experimentos de adsorção em batelada. O biochar foi avaliado e otimizado a partir de um planejamento fatorial fracionário com as variáveis: temperatura de pirólise (500, 600 e 700ºC), tempo de pirólise (30, 105 e 180 minutos) e concentração de cloreto de zinco (5, 12,5 e 20%). Uma capacidade de adsorção em equilíbrio de 78,13 mg.g^{-1} e um rendimento de 26,42% foram obtidos usando 700ºC, 30 min, 12,5%. Este biochar foi aplicado na adsorção de Cr em solução aquosa, sob diferentes velocidades de agitação (100, 150 e 200 rpm). Maior velocidade de agitação reduziu a capacidade de adsorção do biochar de 90 para 72 mg.L^{-1}. Além disso, o equilíbrio de adsorção de Cr foi alcançado antes de 100 min. O modelo de pseudo-primeira ordem melhor descreveu a cinética de adsorção de Cr. O modelo isotérmico de Redlich-Peterson foi o que melhor se ajustou aos dados experimentais, com o parâmetro g (próximo de 1) sugerindo as hipóteses de Langmuir como as mais apropriadas para descrever a adsorção de Cr no carvão ativado otimizado.
Palavras-chave: bioadsorção, remoção de cromo, carvão ativado, resíduo de cervejaria.

INTRODUCTION

The implementation of new brewing industries has increased significantly in recent years (CORDEIRO et al., 2012; SARAIVA et al., 2019). Among the types of waste generated by beer production, Brewer's spent grain (BSG) represents 85% of the total waste produced by the industry (MATHIAS et al., 2014). In general, after the beer fermentation process, approximately 20 kg of BSG is obtained for every 100 L of beer produced, the same being mainly composed of barley grain hulls, which contain cellulose, polysaccharides, lignin, some lipids and polyphenolic components, in addition to proteins, fibers, vitamins, minerals and amino acids (IVANOVA et al., 2017; MUSSATTO et al., 2006).

The large volume of BSG generated by the production process associated with its low cost and its inherent physicochemical characteristics make this residue an attractive biotechnological raw material to be used for the most varied purposes (SARAIVA et al., 2019). Currently within the scope of the research, many alternatives have been proposed for the use of BSG in the most varied segments, such as in the feeding of animals and ruminants, production of breads and hamburgers, production of biodegradable

Received 12.28.21 Approved 12.16.22 Returned by the author 01.26.23
CR-2021-0914.R3
Editors: Leandro Souza da Silva Tales Tiecher

foams, among others (ALIYU & BALA, 2011; MELLO & MALI 2014; KTENIOUDAKI et al., 2012; SARAIVA et al., 2019).

In addition to these applications, the production of activated carbon (AC), currently known as biochar from BSG has emerged as a promising alternative for the use of this waste (VANDERHEYDEN et al., 2018; GONÇALVES et al., 2017; MACHADO et al., 2020). In a recent study, LOPES et al. (2021) optimized the parameters involved in the preparation of biochar from BSG through physical activation and showed that BSG is a potential precursor highly available and ecologically correct to be used with a biochar. In addition, biochar from BSG has shown high rates of adsorption of organic matter and organic compounds such as paracetamol (NADOLNY et al., 2020).

However, the process of preparing the biochar is essential for the adsorption performance (WONG et al., 2018). The preparation processes can be of chemical and physical order. In the chemical activation process, the activator, which may be acid, alkali and some salts, are mixed with the precursor material of the biochar and pyrolyzed at temperatures varying between 500 to 900 ºC. Meanwhile, during physical activation, oxidizing gases (CO_2, air), steam or a mixture of them are used together with the precursor material that is heated at temperatures between 800 and 1000 ºC (MARSH, 2006). Both activations have advantages and disadvantages (WONG et al., 2018). Therefore, chemical activation exclusively for the case of BSG seems to offer advantages over physical activation.

Factors such as time and temperature of pyrolysis are essential factors for obtaining a biochar with a high adsorptive capacity (SCHETTINO et al., 2007). The effect of these variables on the surface area, the adsorption capacity and the pore volume have been studied (LOPES et al., 2021). However;although, currently BSG is commonly used as a precursor to biochar, when it comes to chemical activation, it is not known what are the optimized conditions that result in good adsorption performance for this material.

Significant Cr—effluents are generated from electroplating industry, leather processing, oil refineries, textile industries, ceramic plants and other industrial processes, whereas CrIII and CrVI are the main species found in aqueous environment (KARRI et al., 2020; RODRIGUES et al., 2020). Cr III causes risks to human health, as well as negative environmental impacts. For human health, Cr is considered a toxic and carcinogenic metal, which can cause chemical pneumonia, perforation in the nasal septum, lung cancer and dermatitis (WANG et al., 2011). While for the environment, Cr III causes pollution of surface water bodies, being lethal for aquatic organisms and causing death for terrestrial biota (ADRIANO, 1986). At the same time, Cr III, an essential trace element in mammalian metabolism, exhibits lower toxicity and mobility (MOHAN, 2006). In addition, it is important to note that in Brazil, the current legislation regarding the standards for effluent disposal into surface water bodies presents restrictive values in relation to the concentrations of Cr (0.05 $mg.L^{-1}$) (BRASIL, 2019).

Due to the fate and the need of Cr removal from aqueous environment, the development of alternative and cheap Cr removal techniques such as adsorption have been developed. BSG has attracted attention as a potential matrix for biochar production to be further used as adsorbent. In this sense, this research proposed to evaluate the conditions of biochar production from BSG and the efficiency of Cr adsorption through kinetics, isotherm, and thermodynamic studies.

MATERIALS AND METHODS

BSG preparation

The wet BSG was supplied by a beer producer located in the city of Videira, in the state of Santa Catarina, located at 27º00’30” S and 51º09’06” W, Brazil. First, the BSG was washed and then dried in an oven for 24 h, at a temperature of 105 ºC, crushed into particles with diameters ranging between 250 and 425 µm, and stored in amber flasks until the moment of use. The moisture content, the volatile matter, ash and fixed carbon content were estimated via centesimal analysis, following recommendations of the American Society for Tests and Materials (ASTM - D1762-84).

Biochar production optimization

To produce the biochar, the BSG was initially impregnated with the activating agent ($ZnCl_2$) and submitted to constant agitation at 25ºC, for 24 hours. Then, after maintaining the pH of the samples close to neutrality, they were dried at 105 ºC for 6 h and stored, prior to the pyrolysis process. Pyrolysis was carried out in a muffle furnace.

A full factorial design was applied to evaluate the combination of the factor influencing the biochar preparation. The Box-Behnken matrix of 23 factorial design was performed for 15 runs. The pyrolysis temperature (500, 600 and 700ºC),

pyrolysis time (30 105 and 180 minutes) and $ZnCl_2$ concentration (5, 12.5 and 20%) were the evaluated factors, and their levels and central values are detailed table 1. The combined effects for the tested parameters for the biochar preparation were evaluated according to the response parameters named: surface area ($m^2.g^{-1}$), yield (%) and adsorption capacity ($mg.g^{-1}$), with the same experimental conditions used for the preliminary adsorption experiment above described.

Statistica (StatSoft, USA) software was used for the experimental design, with a randomized experimental order to avoid systematic mistakes. A 2-way interaction between factors was used to calculate the model, at 95% of confidence level. Factors or their combinations resulting in p-values higher than 0.05 were discarded. Significant effects, those considered for the model and that most influenced the response, were evaluated by analysis of variance (ANOVA) at 95% confidence from Fisher test (F-value) and p-values. The parameter is significant if $P < 0.05$.

Biochar characterization

The biochar was characterized according to its surface area, pore volume, and apparent density using N_2 adsorption isotherms at 77 K using a Quantachrome® analyzer (Nova 1200e). The specific area was calculated according to the Brunauer-Emmet-Teller (BET) method (BRUNAUER et al. 1938), and the volume of the micropores was calculated by the t-plot method and the distribution of the mesopores was determined by the BJH method (BARRETT, et al. 1951). In addition, the biochar was also characterized by scanning electron microscopy (SEM) (JEOL JSM 6360-LV). The samples were fixed on supports, using a copper tape and metallized with a thin layer of gold in the metallization device (SCD 050 from the Bal-Tec brand), using 40 milliamps for 2 minutes.

Biosorption studies

Preliminary adsorption experiment

The preliminary adsorption experiments to select the best biochar preparation conditions were performed in Erlemeyer flasks filled with 300 mL of a 100 $mg.L^{-1}$ $Cr(NO_3)_3$ solution at pH 5.0 and 0.25g of biochar. The flasks were maintained at 25ºC and stirred at 150 rpm during 24 hours. The Cr concentration was measured using an atomic absorption spectrophotometer (AA 500 PG instruments). The solution pH and adsorbent dosage were parameters previously defined (data not published).

Adsorption kinetics

The adsorption kinetics experiments were performed as follows: 30 $mg.L^{-1}$ Cr at pH 5.0; 0.25g of biochar and 25ºC in a reciprocal shaking. Samples were collected each 5 minutes until 180 minutes of testing, in order to ensure sufficient time for the system to reach equilibrium. Homogeneous samples were collected to maintain the biochar/solution ratio, followed by centrifugation to remove biochar and to

Table 1 - Experimental design with real and coded levels and the experimental responses values.

Run	Pirolysis temperatura (^{0}C)	Pirolysis time (min)	$ZnCl_2$ (%)	Surface area ($m^2.g^{-1}$)	Yield (%)	Adsorption capacity ($mg.g^{-1}$)
1	-1 (500)	-1 (30)	0 (12.5)	393	18.43	38.33
2	+1 (700)	-1 (30)	0 (12.5)	412	26.42	78.13
3	-1 (500)	+1 (180)	0 (12.5)	392	17.34	27.33
4	+1 (700)	+1 (180)	0 (12.5)	284	16.53	28.13
5	-1 (500)	0 (105)	-1 (5)	298	18.52	30.12
6	+1 (700)	0 (105)	-1 (5)	285	16.2	21.2
7	-1 (500)	0 (105)	+1 (20)	288	19.32	20.12
8	+1 (700)	0 (105)	+1 (20)	399	20.43	68.9
9	0 (600)	-1 (30)	-1 (5)	287	16.54	29.4
10	0 (600)	+1 (180)	-1 (5)	312	15.44	26.5
11	0 (600)	-1 (30)	+1 (20)	401	18.12	72.2
12	0 (600)	+1 (180)	+1 (20)	292	16.44	23.15
13	0 (600)	0 (105)	0 (12.5)	320	16.16	30.2
14	0 (600)	0 (105)	0 (12.5)	302	18.12	31.3
15	0 (600)	0 (105)	0 (12.5)	312	17.2	29.8

measure Cr concentration as immediately identified by means of the atomic absorption spectrophotometer. To assess the influence of agitation, three different agitation speeds were evaluated (100, 150 and 200 rpm). The adsorption capacity (qt) over time t (t) was determined using Equation 1 (DALL'AGNOL et al., 2022).

$$q_t = \left(\frac{C_0 - C_t}{m}\right)V \quad (1)$$

Where: qt: represents the amount of metal adsorbed at time t (mg.g^{-1}); v: the volume of the solution (L); Co and Ct: absorbate concentrations (mg.L^{-1}) in the initial time and time t, respectively; m: mass of the adsorbent (g).

Nonlinear kinetic models were tested to describe the adsorption of the metal (LAKSACI et al., 2017). The nonlinear models of pseudo-first order (PFO), pseudo-second order (PSO) and Elovich used are expressed in table 2.

Isotherm equilibrium and themodynamics

The adsorption equilibrium isotherms were performed at different temperatures (25, 35 and 45 ºC) with different Cr concentrations (5, 10, 15, 20, 30 mg.L^{-1}), using 0.25 g of biochar which resulted in the highest adsorption capacity of 78.13 mg g^{-1} (700ºC pyrolysis temperature, 30 min pyrolysis time, 12.5% ZnCl concentration). The solutions were stirred at 120 rpm for 180 min. After this, the samples were centrifuged and the Cr concentration was assessed by reading on an atomic absorption spectrophotometer (AA 500 PG instruments). The adsorption capacity at equilibrium time was determined using Equation 2 (DALL'AGNOL et al., 2022).

$$q_e = \left(\frac{C_0 - C_e}{m}\right)Vq_e = \left(\frac{C_0 - C_e}{m}\right)V \quad (2)$$

Where, q_e: represents the amount of metal adsorbed at equilibrium (mg.g^{-1}); Ce: final concentration of the adsorbate in solution at equilibrium (mg.L^{-1}); Co: the adsorbate concentration (mg.L^{-1}) in the initial time, V: the volume of the solution (L); m: mass of the adsorbent (g).

Nonlinear equations were applied to best describe the adsorption equilibrium using the isothermal models of Langmuir, Freundlich, Redlich-Peterson and Temkin models, as presented in table 2. The thermodynamic properties including Gibbs free energy, enthalpy and entropy were determined through the van't Hoff equation and expressed according to Equations 3 and 4.

Table 2 - Kinetic and isothermal models and non-linear equations.

Models	Non-linear equations	Reference
Pseudo-first order (PFO)	$q_t = q_e(1 - e^{-K_1 t})$	(LAGERGREN, 1898)
Pseudo-second order (PSO)	$q_t = \frac{K_2 q_e^2 t}{1 + K_2 q_e t}$	(HO & MCKAY, 1999)
Elovich	$q_t = \frac{1}{\beta} ln\,(1 + \alpha\,\beta\,t)$	(ROGINSKY & ZELDOVICH, 1934)
Langmuir	$q_e = \frac{q_m K_L C_e}{1 + K_L C_e}$	(LANGMUIR, 1918)
Freundlich	$q_e = K_F C_e^{\frac{1}{n}}$	(FREUNDLICH, 1906)
Redlich-Peterson	$q_e = \frac{K_R C_e}{1 + a_R C_e^b}$	(REDLICH & PETERSON, 1959)
Temkin	$qe = \frac{RT}{b_t}\ln(K_t . C_e)$	(TEMKIN & PYZHev, 1939)

q_t = adsorption capacity at time t (mg.g^{-1}); q_e = adsorption capacity at the equilibrium (mg g^{-1}); t = time (min); K_1 and K_2 = PFO (min $^{-1}$) and PSO (g mg^{-1}.min^{-1}) constants; α = initial value of the adsorption rate (g.mg^{-1}.min^{-1}); β = desorption coefficient (g.mg^{-1}); q_m = monolayer sorption capacity (mg.g^{-1}); K_L = Langmuir constant (L mg^{-1}); C_e = concentration at the equilibrium (mg.L^{-1}); K_F = Freundlich constant (mg g^{-1}); 1/n = heterogeneity constant; K_R (L.g^{-1}) a_R and b = Redlich–Peterson constants (0 < b < 1); R = ideal gases constant (8.3144 J mol^{-1} K^{-1}); T = temperature (ºK); K_T = Temkin equilibrium constant (L.g^{-1}); Ce = fluid bed equilibrium constant; b = adsorption heat constant (J.mol^{-1}).

$$ln\ K_{ads} = \frac{\Delta Sads}{R} - \frac{\Delta Hads}{RT} \quad (3)$$

$$\Delta G_{ads} = \Delta H_{ads} - T\ \Delta S_{ads} \quad (4)$$

Where, ΔG_{ads}: Gibbs free energy (kJ mol^{-1}); R: universal gas constant (8.314 J mol^{-1} K^{-1}); T: temperature (K); ΔH°ads: enthalpy in adsorption (J mol^{-1}); ΔS°ads: adsorption entropy (J mol^{-1}).

The models that showed the highest values for determining the correlation coefficient (R^2) and the lowest values for the normalized standard deviation (Δq) were considered the best to describe the kinetic and isothermal adsorption curves (Equation 5).

$$\Delta q = 100\sqrt{\frac{\sum\left[\frac{(q_{,exp} - q_{,cal})}{q}, q_{exp}\right]^2}{N-1}} \quad (5)$$

Where: N is the total number of experiments, qcal and qexp are the calculated and experimental adsorption capacities in equilibrium (qe) (isotherms) or at each time t (qt) (kinetic curves), respectively.

The nonlinear regressions and plots for the kinetic and isotherm models were performed using the software Origin® 2017 (ORIGINLAB CORPORATION, USA).

RESULTS AND DISCUSSION

BSG and Biochar characterization

The percentage of humidity, volatile matter, ash and fixed carbon of BSG were 9.0%, 82.8%, 2.3% and 12.4%, respectively. Similar values were reported by Lopes et al. (2021) using a BSG obtained from a local brewery located in south Brazil, for humidity (7.03%), volatile matter (79.42%), ash (1.68%) and fixed carbon (11.87%). This behavior showed that BSG does not show great variation in relation to the local production characteristics of each brewery.

The biochar which resulted in the highest adsorption capacity, as presented in the next section, have an average pore diameter and pore volume of 1.44 nm and 0.27 $cm^3.g^{-1}$, and a surface area of 412 m^2 g^{-1}. Sing et al (1985) indicated a classification according to pore size. Pores with widths exceeding about 50 nm (0.05m) are called macropores. Pores with widths not exceeding about 2 nm are called micropores and pores of intermediate size are called mesopores. In this way, results showed the predominance of micropores.

However, in the SEM images presented figure 1, it is possible to observe micropores ranging from 10 to 150 µm. This heterogeneous pore sizes are also observed for activated carbon when adsorbing 2-phenylethanol (CARPINÉ et al., 2013). It was possible to identify in the BSG an irregular and rough structure, characteristic of a structure arrangement of vegetable raw material (YOKOYAMA et al., 2019). After the process of preparing and obtaining the biochar, the surface of the charcoal showed significant changes with greater heterogeneity of the particles, as well as channels which can be associated with internal pores.

Optimization of Biochar from BSG

In general, the highest adsorption capacity was obtained with higher pyrolysis temperature (700

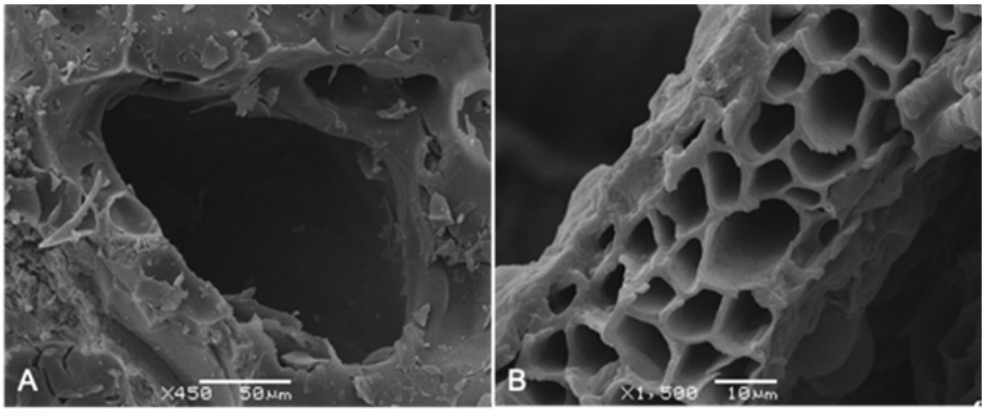

Figure 1 - SEM images at 450x (A) and 1.500x (B) of the biochar under the conditions defined as ideal for the adsorption process.

ºC), lower pyrolysis time (30 min) and middle $ZnCl_2$ concentration (12.5 %) (Table 1). Higher pyrolysis temperatures may cause the decomposition of organic compounds in the precursor material, resulting in greater pore formation and, consequently, a greater surface area of the biochar (MOHANTY et al., 2005; LENG et al., 2021). Previous studies conducted in biochar originating from tomato processing residues, also activated with $ZnCl_2$, showed that the increase in the temperature of pyrolysis (from 400 to 600 ºC) generated an increase in its surface area from 648 to 1093 $m^2.g^{-1}$ (SAYGILI & GUZEL, 2016).

Moreover, the highest adsorption capacity was identified together with the highest values of surface area (412 $m^2.g^{-1}$). According to Weber & QUICKER (2018), larger and accessible surface area are key features for biochar reactivity. MACHADO et al. (2020) showed that a larger surface area of the biochar from BSG caused a greater adsorption performance. The authors showed specific surface area values close to 545 $m^2 g^{-1}$ and 161 $m^2 g^{-1}$ for $ZnCl_2$-activated biochar and CO_2-activated biochar, respectively. These values were extremely higher in relation to the biochar without activation (6.5 $m^2 g^{-1}$), and confirmed that the activation efficiently performed.

The Pareto diagram showed that almost all the tested parameters were statistically significant, even with linear or quadratic interactions, at a confidence level of 95%, for the adsorption capacity response (Figure 2). The pyrolysis time and the $ZnCl_2$ mostly influenced the surface area of the biochar. Moreover, the isolated pyrolysis temperature has no significant influence over the biochar surface area but, its combined effect with pyrolysis time and $ZnCl_2$ was significant. At the temperatures around

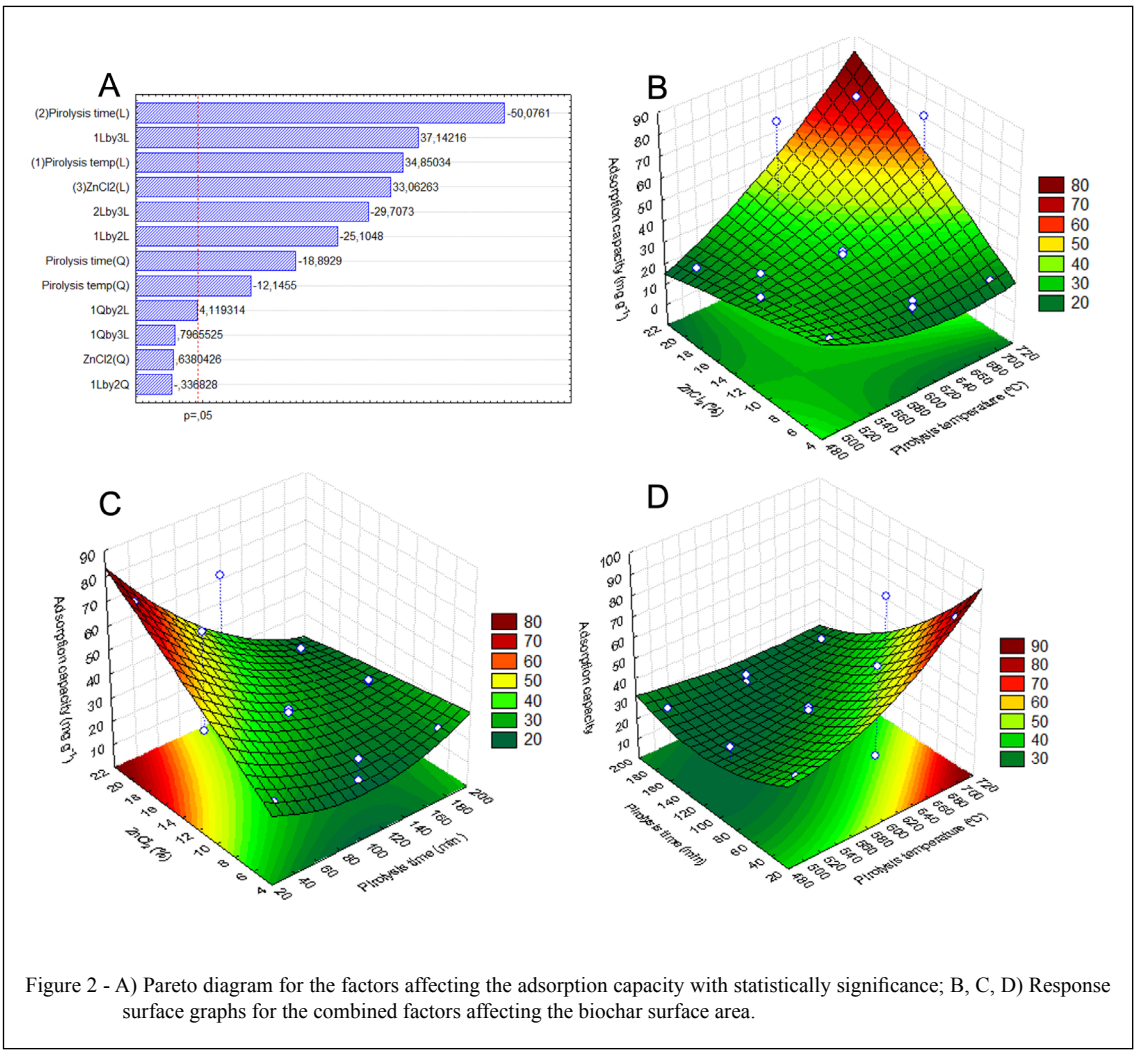

Figure 2 - A) Pareto diagram for the factors affecting the adsorption capacity with statistically significance; B, C, D) Response surface graphs for the combined factors affecting the biochar surface area.

500ºC amorphous carbons is transformed into crystalline carbons via condensation, more volatiles are removed, creating sparse regions, which leads to cracks in the material, and thereby generating mesopores (KEILUWEIT et al., 2010). Micropores exert the greatest effect on the surface area, whereas the value of total pore volume is positively correlated to the pore size (LENG et al., 2021). Moreover, activating agent concentration is directly linked to the dilation of the pores, i.e., the higher the concentration of $ZnCl_2$ the greater the porous area. However, pore widening will result in a larger total pore volume but a lower surface area (LENG et al., 2021; MIAO et al., 2013). In this way, the surface response showed that higher pyrolysis time combined with lower $ZnCl_2$ concentration led to higher biochar surface area.

Adsorption kinetics

The experimental data were evaluated using the non-linear adjustments of PFO, PSO, and the Elovich models (Table 3). According to the figure 3, the equilibrium time was reached after approximately 100 minutes for those experiments with agitation rates of 150 and 200 rpm. In the case of the stirring rate of 100 rpm, equilibrium was reached around 130 minutes of testing. The agitation rate clearly influenced the adsorption kinetics since different adsorption capacities were achieved for each agitation rates.

For the experimental data, the Elovich model fitted best with higher correlation coefficients ($R^2 > 0.98$) and the lowest Δq (< 4.85), for all the tested agitation speed. The Elovich model suggested that the adsorption is regarded to chemical bonds between the Cr and the adsorbent. Also, the increasing in agitation rate increased the initial adsorption rate (α) from 10.82 ± 0.52 to 349.7 ± 142.8 $g.mg^{-1}.min^{-1}$, showing how this parameter influenced the adsorption process.

The PSO model for the 100 rpm experiment presented the closest adjusted qe values (93.3 ± 1.8 $mg.g^{-1}$) to the experimental qe (87.6 $mg.g^{-1}$), with lower qe standard deviation and higher R^2 when compared to the PFO model; although, this model also represented well the experimental data. The same result was found by Ramos et al. (2016), using carboxylate-functionalized sugarcane bagasse to adsorb copper (II), with k^2 value 0.154 $g.mmol.min^{-1}$.

Other studies carried out with different materials (soil, red mud) used for adsorption of Cr were better adjusted with the PFO model (GUPTA et al., 2001; RENGARAJ, et al., 2002). The k_1 PFO rate constant refers to how fast the Cr adsorption occurred, and their value ranged from 0.01 to 0.03 min^{-1}.

Equilibrium isotherms and thermodynamics

The adsorption isotherms parameters together with the thermodynamic analysis allow the understanding of the surface properties, interaction mechanisms and the affinity degree of the biochar and the Cr. The equilibrium isotherms are also used to calculate the maximum adsorption capacity in the tested conditions (AL-GHOUTI & DA'ANA, 2020; BENI & ESMAEILI 2020). Equilibrium is achieved when the adsorbent and adsorbate are in contact for long enough to establish a dynamic balance between the concentration of the solution

Table 3 - Parameters calculated from the nonlinear fits of kinetic models to the experimental data.

Agitation (rpm)	$q_{e,exp}$ ($mg.g^{-1}$)	Pseudo-first order	Pseudo-second order	Elovich
100	87.6	q_e= 80.95 ± 1.88	q_e= 93.35 ± 1.84	α = 10.82 ± 0.52
		k_1= 0.039 ± 0.004 R^2_{adjust} = 0.932	k_2= 5.42 x 10^{-4} ± 5.51 x 10^{-5}	β = 0.05 ± 8.93 x 10^{-4}
		Δq= 10.5	R^2_{adjust}=0.978	R^2_{adjust} =0.998
			Δq= 8.56	Δq = 3.37
150	90.3	q_e= 84.59 ± 2.01	q_e= 93.62 ± 1.86	α = 38.82 ± 3.73
		k_1 = 0.058 ± 0.007	k_2 = 9.32×10^{-4} ± 1.78×10^{-4}	β = 0.064 ± 0.002
		R^2_{adjust} = 0.961	R^2_{adjust}=0.961	R^2_{adjust}= 0.993
		Δq= 9.32	Δq= 5.67	Δq= 4.85
200	72.4	q_e = 64.08 ± 1.60	q_e = 68.71 ± 1.52	α = 349.7 ± 142.8
		k_1 = 0.163 ± 0.03	k_2 = 0.003 ± 7.279 x 10^{-4}	β = 0.127 ± 0.007
		R^2_{adjust} = 0.797	R^2_{adjust} = 0.907	R^2_{adjust} = 0.980
		Δq= 12.49	Δq= 7.09	Δq= 4.13

*Δq = %.

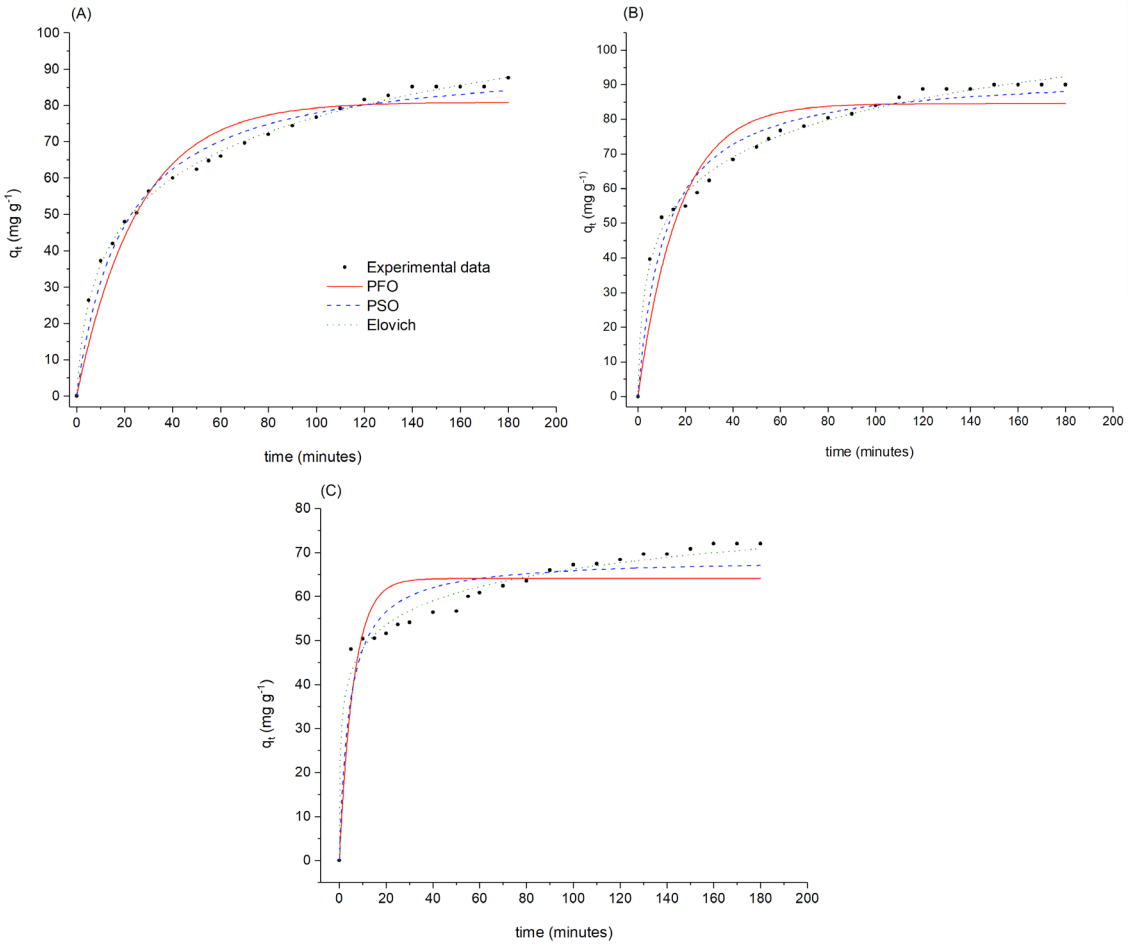

Figure 3 - Adsorption kinetic curves obtained from initial Cr concentrations of 30 mg.L^{-1}. A) 100 rpm, B) 150 rpm, C) 200 rpm, as well as the non-linear fits of PFO, PSO and Elovich models.

volume and the interface concentration (GUPTA & BHATTACHARYYA, 2011). The figure 4 shows the adsorption isotherms of Cr obtained at different temperatures (25, 35 and 45 °C), adjusted according to the non-linear models of Langmuir, Freundlich, Redlich-Peterson and Tempkin.

The adjustment of the Langmuir model to the experimental data obtained under the different temperatures showed an R^2 ranging from 0.92 to 0.98 and a Δq with values ranging from 3.70 to 4.39. This model reflects the monolayer adsorption on a surface with energetically equivalent sites, where there is no lateral interaction or steric impediment between the adsorbed molecules (GUPTA et al., 2001; GUPTA & BHATTACHARYYA, 2011).

According to the table 4, the maximum Cr adsorption capacity (Qm) increased considerably (from 31.8 to 64.6 mg.g^{-1}) with the increase in temperature, indicating that the increase in temperature favored the adsorption process. The maximum adsorption capacity is influenced by several factors such as, for example, the characteristics of the activated charcoal (AC), the type of adsorbate and the conditions of the solution (FOO & HAMEED, 2010). Previous studies showed that the Qm can vary between 22.31 to 199.7 mg.g^{-1} (Table 5). Based on the results obtained, the biochar used in this study has good adsorption capacity.

The adjustments of the Freundlich model provided a value of R^2 (0.79 to 0.88) and Δq (5.65 to 9.15%) lower than the comparison with the Langmuir model (Table 6). The empiric Freundlich model does not represent the maximum adsorption capacity and does not present the equilibrium plateau, not fitting well the final experimental points of the equilibrium curve (SOUZA et al., 2021).

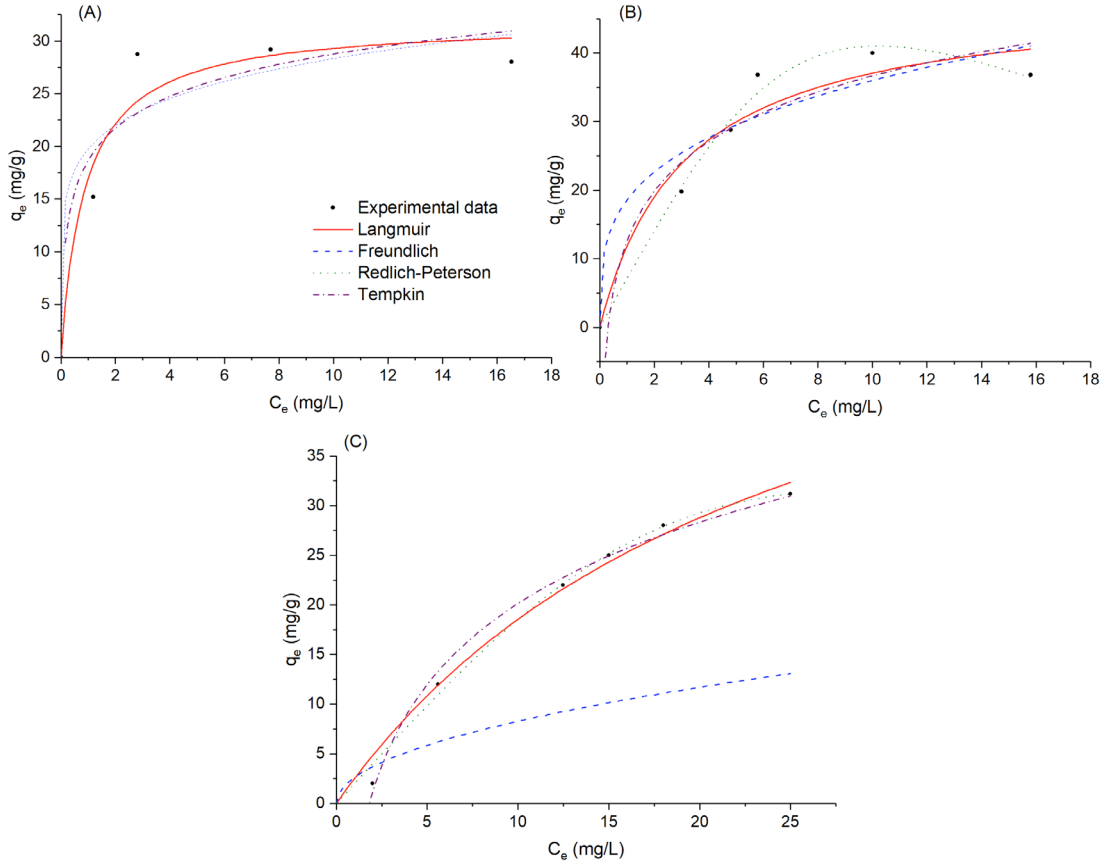

Figure 4 - Adsorption isotherms obtained at temperatures of 25°C (A), 35ºC (B), and 45 ºC (C), as well as the nonlinear fits of Langmuir, Freundlich Redlich-Peterson and Temkin models.

The Temkin model showed R^2 values from 0.87 to 0.99 and Δq from 2.12 to 6.78 (Table 6). This model considers that the heat of adsorption of all molecules in the layer decreases linearly with the coverage of the adsorbent surface (Foo & Hameed, 2010). The Redlich-Peterson model showed the best fit for the experimental data, with the highest R^2 (0.97 to 0.99) and the lowest Δq value (1.66 to 3.48) (Table 6). This model presents similar premises presented by the Langmuir and Freundlich models. The exponent g can assume interval values between 0 to 1, where at the limit of g is 0, the most appropriate model is the Freundlich model. On the other hand, if the value of g is close to 1, the most suitable model is Langmuir's (BRDAR et al., 2012). From the values of g (0.87 to 0.89) identified in this study, the evidence fits from the Redlich-Peterson model that the adsorption of Cr is best described by Langmuir's assumptions.

The thermodynamic parameters were calculated considering the Langmuir model, as presented in table 7 and figure 5. It can be seen in table 7 that change in the Gibbs free energy (ΔG) are negative for all the tested temperatures, indicating that the adsorption process is spontaneous and favorable. According to the Langmuir model, higher temperature increased the adsorption capacity. The positive enthalpy is considered for endothermic reactions. The slightly positive value obtained in this study (3.07 $kJ.mol^{-1}$) suggested a physisorption reaction (SOUZA et al., 2021). The change in the entropy (ΔS) indicated the randomness of the reaction at the solid/liquid interface. The positive entropy reveals the system disorder and randomness.

Environmental application of BSG biochar for Cr removal

The state of Santa Catarina has the highest number of breweries per inhabitants in Brazil, according to the ministry of agriculture (BRASIL, 2019). Most of micro and craft

Table 4 - Parameters calculated from the nonlinear fits of theoretical isotherm models to the experimental data of Cr adsorption onto activated carbon.

Models	Temperature		
	25 °C	35 °C	45 °C
	Langmuir		
q_m	31.88 ± 3.39	48.58 ± 7.35	64.60 ± 11.73
K_L	1.13 ± 0.60	0.32 ± 0.15	0.04 ± 0.012
R^2	0.927	0.927	0.986
Δq_e	4.39	4.75	3.70
	Freundlich		
K_F	19.78 ± 3.92	18.56 ± 4.82	22.12 ± 8.855
n_F	6.36 ± 3.95	3.47 ± 1.45	4.78 ± 2.86
R^2	0.861	0.888	0.798
Δq_e	6.04	5.65	9.15
	Redlich-Peterson		
K_{RP}	17.64 ± 4.21	7.18 ± 0.66	1.999 ± 0.23
a_{RP}	0.206 ± 0.14	0.004 ± 0.004	$4.59x10^{-4}$ ± 0.001
g	0.89 ± 0.18	0.87 ± 0.40	0.88 ± 0.95
R^2	0.971	0.984	0.991
Δq_e	3.48	2.64	1.66
	Temkin		
b	603.4 ± 310.14	253.0 ± 86.7	224 ± 8.08
A	70.531 ± 211.69	3.338 ± 3.60	0.551 ± 0.37
R^2	0.876	0.907	0.995
Δq_e	6.78	5.45	2.12

*Δq = %.

breweries are in south and southeast of Brazil (80%), whereas Santa Catarina state accounts for 13%. In this way, the region is a potential BSG producer, which requires correct management and disposal, frequently associated to costs for the breweries. Alternative use of this residue may result in environmental benefits and reduction for BSG disposal.

Besides BSG production potential and the need to reuse this residue, Santa Catarina also attract attention due to the heavy metal contamination of water bodies, such as Cr. Cr is widely used in chemical industry for various applications such as pigments, metal plating, metallurgy, and in chemical production. Cr was detected up to 95.8 mg kg^{-1} of sediment samples in an estuarine region

Table 5 - Langmuir's adsorption capacity (qm) for Cr adsorption into varied biochar materials.

Adsorbent	q_m ($mg.g^{-1}$)	Experimental conditions	Reference
Actived carbon	199.7	55 ºC; pH 3.0; d = 1.0 g L^{-1}	LOPES et al., (2021)
Fe_3O_4-activated carbon	22.31	25 ºC; pH 5.88; d = 1.0 g L^{-1}	CAZETTA et al. (2016)
Cu:ZnS-NPs-Actived carbon	85.4	25 ºC; pH 6.0	AGARWAL et al. (2016)
Modified chitin	93.3	55 ºC; pH 4.0	LIMA et al., (2009)
Carboxylated-functionallized sugarcane bagasse	69.40	25 ºC; pH 5.5 d = 1.0 g L^{-1}	RAMOS et al., (2016)
Zinc-modified sugarcane bagasse	>200	25 ºC; pH 5.5 d = 2.0 g L^{-1}	GAO et al., (2015)
Steam activated macroalgae biomass	137	25 ºC; pH 5.5 d = 0.1 g L^{-1}	KIM et al., (2016)

Note: d = adsorbent dosage.

Table 6 - Analysis of variance (ANOVA) of quadratic regression model for surface area as experimental response.

Parameters	SQ	DF	MS	F-value	P-value
(1)Pirolysis temperature(L)	1198.775	1	1198.775	1986.919	0.000503
Pirolysis temperature(Q)	0.239	1	0.239	0.396	0.593555
(2)Pirolysis time (min)(L)	2045.375	1	2045.375	3390.125	0.000295
Pirolysis time (min)(Q)	383.571	1	383.571	635.754	0.001569
(3)ZnCl2 (%)(L)	269.197	1	269.197	446.183	0.002234
ZnCl2 (%)(Q)	214.650	1	214.650	355.773	0.002799
1L by 2L	380.250	1	380.250	630.249	0.001583
1L by 2Q	288.331	1	288.331	477.897	0.002086
1Q by 2L	162.140	1	162.140	268.740	0.003700
1L by 3L	832.323	1	832.323	1379.540	0.000724
1Q by 3L	47.274	1	47.274	78.354	0.012523
2L by 3L	532.456	1	532.456	882.523	0.001131
Error	1.207	2	0.603		
Total SS	5194.590	14			
R^2	0.9983				

SQ is the sum of squares; DF is the degrees of freedom; MS is the mean for squares.

of the Baía de Babitonga, located in northeast of Santa Catarina, where metallurgical and textile industries are concentrated (SOUZA et al., 2021). Another study presented Cr concentrations up to 16 mg/kg of dry sediment in the same study area (BONATTI et al., 2004).

Cr contamination due to anthropogenic activities like industrial processes may be controlled using end-of-pipe solutions including wastewater treatment technologies, since the pollution source can be identified and controlled. Adsorption has been regarded as a promising technology due to its cheap and efficient nature, when using agro-industrial residues such as BSG. This enables the applicability of this residue, instead of its disposal. In this way, many breweries can value their by-product of their production process, thus reducing costs with final disposal and management.

CONCLUSION

According to this study, higher pyrolysis temperature (700 ºC), lower pyrolysis time (30 min) and higher $ZnCl_2$ concentration (12.5 %) resulted in the biochar with better adsorption capacity (78.13± 0.87 mg.g^{-1}) and higher surface area (412 $m^2.g^{-1}$). Also, 130 minutes were required to reach the equilibrium in the kinetic experiments, which revealed that PSO model best described the Cr adsorption kinetics. Isothermal studies showed that the Langmuir model best fitted to the experimental data, whereas the monolayer adsorption drives the process mechanism. The temperature exerts some effect over the adsorption process. According to this study, BSG biochar has the potential to be applied for adsorption of heavy metals, contributing to the reuse of this residue and the removal of a toxic pollutant from liquid streams.

Table 7 - Thermodynamic parameters of Cr adsorption onto activated carbon.

Temperature	----------Parameters----------		
	ΔG (kJ.mol^{-1})	ΔH (kJ.mol^{-1})	ΔS (J.$mol^{-1}.K^{-1}$)
30	-52.84	3.07	123.58
40	-54.91		
50	-56.12		

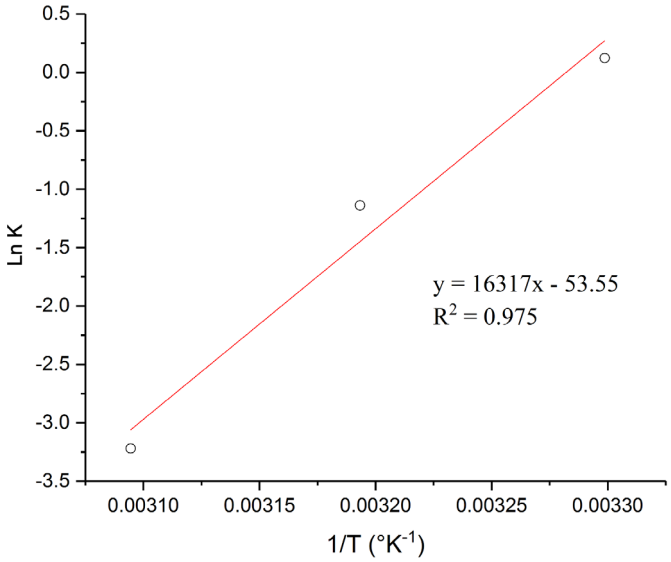

Figure 5 - Van't Hoff plot of Cr adsorption onto activated carbon.

ACKNOWLEDGEMENTS

The authors acknowledge the Universidade do Oeste de Santa Catarina (UNOESC), the Universidade Federal de Santa Catarina (UFSC) and the Universidade Federal do Paraná (UFPR) and was financed in part by the Coordenação de Aperfeiçoamento de Pessoal de Nível Superior (CAPES), Brasil – Finance.

DECLARATION OF CONFLICT OF INTEREST

The authors declare no conflict of interest. The founding sponsors had no role in the design of the study; in the collection, analyses, or interpretation of data; in the writing of the manuscript, and in the decision to publish the results.

AUTHORS' CONTRIBUTIONS

All authors contributed equally for the conception and writing of the manuscript. All authors critically revised the manuscript and approved of the final version.

REFERENCES

ADRIANO DC. **Trace Elements in the Terrestrial Environment**. New York: Springer, 1986.1v.

ASTM D17. **Annual book of ASTM standards** D1762-84, 1984.

ALIYU, S.; BALA, M. Brewer's spent grain: A review of its potentials and applications, **African Journal of Biotechnology**, v.10, p.324–331, 2011. Available from: <https://doi.org/10.4314/AJB.V10I3>. Accessed: Jan. 18, 2021.

AGARWAL, S. et al. Ultrasound-assisted adsorption of Sunset Yellow CFC dye onto Cu doped ZnS nanoparticles loaded on activated carbon using response surface methodology based on central composite design. **Journal of Molecular Liquids**, [S.L.], v.219, p.332-340, 2016. Elsevier BV. Available from: <http://dx.doi.org/10.1016/j.molliq.2016.02.100>. Accessed: May. 02, 2021.

BARRETT, E. P. et al. The Determination of Pore Volume and Area Distributions in Porous Substances. I. Computations from Nitrogen Isotherms. **Journal of The American Chemical Society**, 73, n.1, p.373-380, 1951. American Chemical Society (ACS). Available from: <http://dx.doi.org/10.1021/ja01145a126>. Accessed: Dec. 14, 2020.

BONATTI M. et al .Study of the toxicity of marine sediments of the Babitonga Bay – Brazil. J. Costal Res. 2003. In: **Proceedings of the 8th International Coastal Symposium**, Itajaí, 29. ISSN 0749-0208

BRASIL. 2019. **Ministério da Agricultura, Pecuária e Abastecimento. Secretaria de Defesa Agropecuária**. – Brasília: MAPA/SDA, 2020. 16 p.

BRDAR, M. et al. Comparison of two and three parameters adsorption isotherm for Cr(VI) onto Kraft lignin. **Chemical Engineering Journal**, v.183, p.108-111, fev. 2012. Available from: <http://dx.doi.org/10.1016/j.cej.2011.12.036>. Accessed: Oct. 10, 2021.

BRUNAUER, S. et al. Adsorption of Gases in Multimolecular Layers. **Journal Of The American Chemical Society**, v.60, n.2, p.309-319, fev. 1938. American Chemical Society (ACS).

Available from: <http://dx.doi.org/10.1021/ja01269a023>. Accessed: Nov. 13, 2021.

CARPINÉ, D. et al. Adsorption of volatile aroma compound 2-phenylethanol from synthetic solution onto granular activated carbon in batch and continuous modes. **Journal Of Food Engineering**, v.117, n.3, p.370-377, ago. 2013. Elsevier BV. Available from: <http://dx.doi.org/10.1016/j.jfoodeng.2013.03.008>. Accessed: Jan. 18, 2021.

CAZETTA, L.A. et al. Magnetic Activated Carbon Derived from Biomass Waste by Concurrent Synthesis: efficient adsorbent for toxic dyes. **Acs Sustainable Chemistry & Engineering**, v.4, n.3, p.1058-1068, 2016. American Chemical Society (ACS). Available from: <http://dx.doi.org/10.1021/acssuschemeng.5b01141>. Accessed: Nov. 18, 2021.

CORDEIRO, L.G. et al. Energetic characterization of malt bagasse by calorimetry and thermal analysis. **Journal Of Thermal Analysis And Calorimetry**, [S.L.], v.112, n.2, p.713-717, 2012. Springer Science and Business Media LLC. Available from: <http://dx.doi.org/10.1007/s10973-012-2630-x>. Accessed: Jan. 18, 2021.

DALL'AGNOL, P. et al. Biosorption of Phosphorus Using Alginate-Like Exopolymers: investigation of removal mechanism, kinetic and thermodynamic properties. **Journal of Polymers And The Environment**, [S.L.], v.30, n.2, p.695-706, 2021. Springer Science and Business Media LLC. Available from: <http://dx.doi.org/10.1007/s10924-021-02232-0>. Acessed: Aug. 17, 2021.

FOO, K.y.; HAMEED, B.H. Insights into the modeling of adsorption isotherm systems. **Chemical Engineering Journal**, [S.L.], v.156, n.1, p.2-10, 2010. Elsevier BV. Available from: <http://dx.doi.org/10.1016/j.cej.2009.09.013>. Acessed: Feb. 10, 2021.

FREUNDLICH, H. Over the adsorption in the solution. **The Journal of Physical Chemistry**, v.57, p.385-47, 1906. Acessed: Feb. 10, 2021.

GAO, F. et al. Removal of aqueous ammonium by biochars derived from agricultural residuals at different pyrolysis temperatures. **Chemical Speciation & Bioavailability**, [S.L.], v.27, n.2, p.92-97, 3 abr. 2015. Informa UK Limited. Available from: <http://dx.doi.org/10.1080/09542299.2015.1087162>. Acessed: Oct. 10, 2021.

GONÇALVES, G.C. et.al. Utilization of brewery residues to produces granular activated carbon and bio-oil. **Journal Of Cleaner Production**, [S.L.], v.168, p.908-916, dez. 2017. Elsevier BV. Available from: <http://dx.doi.org/10.1016/j.jclepro.2017.09.089>. Acessed: Apr. 19, 2021.

GUPTA, S. S.; BHATTACHARYYA, K. G. Kinetics of adsorption of metal ions on inorganic materials: a review. **Advances In Colloid And Interface Science**, [S.L.], v.162, n.1-2, p.39-58, fev. 2011. Elsevier BV. Available from: <http://dx.doi.org/10.1016/j.cis.2010.12.004>. Acessed: Aug. 12, 2021.

GUPTA, V. K; et al. Process development for the removal of lead and chromium from aqueous solutions using red mudan aluminium industry waste. **Water Research**, [S.L.], v.35, n.5, p.1125-1134, abr. 2001. Elsevier BV. Available from: <http://dx.doi.org/10.1016/s0043-1354(00)00389-4>. Acessed: Oct. 18, 2021.

HO, Y.S; MCKAY, G. A. kinetic study of dye sorption by biosorbent waste product pith. **Resources, Conservation And Recycling**, [S.L.], v.25, n.3-4, p.171-193, mar. 1999. Elsevier BV. Available from: <http://dx.doi.org/10.1016/s0921-3449(98)00053-6>. Acessed: Oct. 10, 2021.

IVANOVA, K. et al. Extrusion of brewers' spent grains and application in the production of functional food. Characteristics of spent grains and optimization of extrusion. **Journal Of The Institute Of Brewing**, [S.L.], v.123, n.4, p.544-552, 15 ago. 2017. The Institute of Brewing & Distilling. Available from: <http://dx.doi.org/10.1002/jib.448>. Acessed: Jan. 19, 2021.

KARRI, R.R. et al. Improving efficacy of Cr (VI) adsorption process on sustainable adsorbent derived from waste biomass (sugarcane bagasse) with help of ant colony optimization. **Industrial Crops And Products**, [S.L.], v.143, p.111927, jan. 2020. Elsevier BV. Available from: <http://dx.doi.org/10.1016/j.indcrop.2019.111927>. Acessed: Dec. 22, 2020.

KTENIOUDAKI, A. et al. Brewer's spent grain as a functional ingredient for breadsticks. **International Journal Of Food Science & Technology**, [S.L.], v.47, n.8, p.1765-1771, 11 jun. 2012. Wiley. Available from: <http://dx.doi.org/10.1111/j.1365-2621.2012.03032.x>. Acessed: Oct. 10, 2021.

KEILUWEIT, M. et al. Dynamic Molecular Structure of Plant Biomass-Derived Black Carbon (Biochar). **Environmental Science & Technology**, [S.L.], v.44, n.4, p.1247-1253, 25 jan. 2010. American Chemical Society (ACS). Available from: <http://dx.doi.org/10.1021/es9031419>. Acessed: Oct. 10, 2021.

KIM, B et al. Removal of Cu2+ by biochars derived from green macroalgae. **Environmental Science And Pollution Research**, [S.L.], v.23, n.2, p.985-994, 28 mar. 2015. Springer Science and Business Media LLC. Available from: <http://dx.doi.org/10.1007/s11356-015-4368-z>. Acessed: Oct. 24, 2021.

LAGERGREN S. **Zur theorie der sogenannten adsorption gelõster stoffe, Kungliga Svenska Vetenskapsakademiens**. Handlingar, v 24, p.1–39, 1898.

LAKSACI, H. et al. Synthesis and characterization of microporous activated carbon from coffee grounds using potassium hydroxides. **Journal Of Cleaner Production**, [S.L.], v.147, p.254-262, mar. 2017. Elsevier BV. Available from: <http://dx.doi.org/10.1016/j.jclepro.2017.01.102>. Acessed: Oct. 30, 2021.

LANGMUIR, I. THE ADSORPTION OF GASES ON PLANE SURFACES OF GLASS, MICA AND PLATINUM. **Journal Of The American Chemical Society**, [S.L.], v.40, n.9, p.1361-1403, 1918. American Chemical Society (ACS). Available from: <http://dx.doi.org/10.1021/ja02242a004>. Acessed: Sept. 30, 2021.

LENG, L. An overview on engineering the surface area and porosity of biochar. **Science Of The Total Environment**, [S.L.], v.763, p.144204, abr. 2021. Elsevier BV. Available from: <http://dx.doi.org/10.1016/j.scitotenv.2020.144204>. Acessed: Oct. 10, 2021.

LIMA, E. C. et al. A critical review of the estimation of the thermodynamic parameters on adsorption equilibria. Wrong use of

equilibrium constant in the Van't Hoof equation for calculation of thermodynamic parameters of adsorption. **Journal Of Molecular Liquids**, [S.L.], v.273, p.425-434, jan. 2019. Elsevier BV. Available from: <http://dx.doi.org/10.1016/j.molliq.2018.10.048>. Acessed: Nov. 18, 2021.

LOPES, G.K. P.et al Steam-activated carbon from malt bagasse: optimization of preparation conditions and adsorption studies of sunset yellow food dye. **Arabian Journal Of Chemistry**, [S.L.], v.14, n.3, p.103001, mar. 2021. Elsevier BV. Available from: <http://dx.doi.org/10.1016/j.arabjc.2021.103001>. Acessed: Oct. 10, 2021.

MARSH H.; RODRIGUEZ-REINOSO F. **Activated carbon**. Oxford: Elsevir. 2006. 1v.

MATHIAS, T.R.S. et al. Solid wastes in brewing process: A review. **Journal of Brewing and Distilling**. v.5, p.1-9, 2014. Available from: <https://doi.org/10.5897/JBD2014.0043>. Acessed: Oct. 10, 2021.

MELLO, L. R.P.F.; MALI, S. Use of malt bagasse to produce biodegradable baked foams made from cassava starch. **Industrial Crops And Products**, [S.L.], v.55, p.187-193, abr. 2014. Elsevier BV. Available from: <http://dx.doi.org/10.1016/j.indcrop.2014.02.015>. Acessed: Jan. 18, 2021.

MIAO, et. al. Activated carbon prepared from soybean straw for phenol adsorption. **Journal Of The Taiwan Institute Of Chemical Engineers**, [S.L.], v.44, n.3, p.458-465, maio 2013. Elsevier BV. Available from: <http://dx.doi.org/10.1016/j.jtice.2012.12.006>. Acessed: Aug. 18, 2021.

MOHANTY, K.; BISWAS, M.N. Adsorption of phenol from aqueous solutions using activated carbons prepared from Tectona grandis sawdust by ZnCl2 activation. **Chemical Engineering Journal**, [S.L.], v.115, n.1-2, p.121-131, dez. 2005. Elsevier BV. Available from: <http://dx.doi.org/10.1016/j.cej.2005.09.016>. Acessed: Nov. 10, 2021.

MUSSATTO, S.I. et.al. Brewers' spent grain: generation, characteristics and potential applications. **Journal Of Cereal Science**, [S.L.], v.43, n.1, p.1-14, jan. 2006. Elsevier BV. Available from: <http://dx.doi.org/10.1016/j.jcs.2005.06.001>. Acessed: Aug. 10, 2021.

MACHADO, L M.M. et al. Treatment of effluents containing 2-chlorophenol by adsorption onto chemically and physically activated biochars. **Journal Of Environmental Chemical Engineering**, [S.L.], v.8, n.6, p.104473, dez. 2020. Elsevier BV. Available from: <http://dx.doi.org/10.1016/j.jece.2020.104473>. Acessed: Oct. 22, 2021.

MOHAN, D. et al. Activated carbons and low cost adsorbents for remediation of tri- and hexavalent chromium from water. **Journal Of Hazardous Materials**, [S.L.], v.137, n.2, p.762-811, 21 set. 2006. Elsevier BV. Available from: <http://dx.doi.org/10.1016/j.jhazmat.2006.06.060>. Acessed: Oct. 13, 2021.

NADOLNY, B.et al. Use of brewing industry waste to produce carbon-based adsorbents: paracetamol adsorption study. **Journal Of Environmental Science And Health, Part A**, [S.L.], v.55, n.8, p.947-956, 29 abr. 2020. Informa UK Limited. Available from: <http://dx.doi.org/10.1080/10934529.2020.1759320>. Acessed: Dec. 18, 2021.

RAMOS, S. N.C et al. Removal of cobalt(II), copper(II), and nickel(II) ions from aqueous solutions using phthalate-functionalized sugarcane bagasse: mono- and multicomponent adsorption in batch mode. **Industrial Crops And Products**, [S.L.], v.79, p.116-130, jan. 2016. Elsevier BV. Available from: <http://dx.doi.org/10.1016/j.indcrop.2015.10.035>. Acessed: Dec. 18, 2021.

REDLICH, O.; PETERSON, D L. A Useful Adsorption Isotherm. **The Journal Of Physical Chemistry**, [S.L.], v.63, n.6, p.1024-1024, 1 jun. 1959. American Chemical Society (ACS). Available from: <http://dx.doi.org/10.1021/j150576a611>. Acessed: Apr. 18, 2021.

RENGARAJ, S. et al. Removal of nickel from water and synthetic nuclear power plant coolant water by ion exchange resins. **Journal Of Radioanalytical And Nuclear Chemistry**, [S.L.], v.253, n.2, p.241-245, 2002. Springer Science and Business Media LLC. Available from: <http://dx.doi.org/10.1023/a:1019645708495>. Acessed: Apr. 18, 2021.

RODRIGUES, S. K. et al. Changes in Cd and Zn distribution in sediments after closure of an electroplating industry, Sepetiba bay, Brazil. **Marine Pollution Bulletin**, [S.L.], v.161, p.11758, dez. 2020. Elsevier BV. Available from: <http://dx.doi.org/10.1016/j.marpolbul.2020.111758>. Acessed: Apr. 18, 2021.

ROGINSKY, S,Z.; ZELDOVICH, J. The catalytic oxidation of carbon monoxide on manganese dioxide. **Chemcatchem**.v.1, p.554, 1934. Acessed: Apr. 18, 2021.

SARAIVA, B.R. Effect of brewing waste (malt bagasse) addition on the physicochemical properties of hamburgers. **Journal of Food Processing And Preservation**, [S.L.], v.43, n.10, p.1-3, 31 jul. 2019. Wiley. Available from: <http://dx.doi.org/10.1111/jfpp.14135>. Acessed: Apr. 18,2021.

SAYGILI, H.; GÜZEL, F. High surface area mesoporous activated carbon from tomato processing solid waste by zinc chloride activation: process optimization, characterization and dyes adsorption. **Journal Of Cleaner Production**, [S.L.], v.113, p.995-1004, fev. 2016. Elsevier BV. Available from: <http://dx.doi.org/10.1016/j.jclepro.2015.12.055>. Acessed: Apr. 18,2021.

SCHETTINO J. et al. Preparação e caracterização de carvão ativado quimicamente a partir da casca de arroz. **Química Nova**, [S.L.], v.30, n.7, p.1663-1668, 2007. FapUNIFESP (SciELO). Available from:<http://dx.doi.org/10.1590/s0100-40422007000700031>. Acessed: Apr. 18,2021.

SING, K. S. W. et al. Reporting physisorption data for gas/solid systems with special reference to the determination of surface area and porosity (Recommendations 1984). **Pure And Applied Chemistry**, [S.L.], v.57, n.4, p.603-619, 1 jan. 1985. Walter de Gruyter GmbH. Available from: <http://dx.doi.org/10.1351/pac198557040603>. Acessed: Apr. 19, 2021.

SOUZA, F.M. et al. Macrobenthic Community responses to multiple environmental stressors in a subtropical estuary. **PeerJ**, v. 9, p. 12427. Available from: <https://peerj.com/articles/12427>. Acessed: Apr. 18, 2021.

TEMKIN, M.; PYZHEV, V. Kinetics of the synthesis of ammonia on promoted iron catalysts. The Journal of Physical Chemistry, v.13, p.851–867, 1939. Acessed: Jan. 18, 2021.

VANDERHEYDEN, S. R. H. et al. Chromium(VI) removal using in-situ nitrogenized activated carbon prepared from Brewers' spent grain. **Adsorption**, [S.L.], v.24, n.2, p.147-156, 13 dez. 2017.

Springer Science and Business Media LLC. Available from: <http://dx.doi.org/10.1007/s10450-017-9929-7>. Acessed: Jan. 18, 2021.

WANG, Zhen-Xing. et al. Environmental impact and site-specific human health risks of chromium in the vicinity of a ferro-alloy manufactory, China. **Journal Of Hazardous Materials**, [S.L.], v.190, n.1-3, p.980-985, jun. 2011. Elsevier BV. Available from: <http://dx.doi.org/10.1016/j.jhazmat.2011.04.039>. Acessed: Apr. 18, 2021.

WEBER, K.; QUICKER, P. Properties of biochar. **Fuel**, [S.L.], v.217, p.240-261, abr. 2018. Elsevier BV. Available from: <http://dx.doi.org/10.1016/j.fuel.2017.12.054>. Acessed: Apr. 18, 2021.

WONG, S. et al. From pollutant to solution of wastewater pollution: synthesis of activated carbon from textile sludge for dye adsorption. **Chinese Journal Of Chemical Engineering**, [S.L.], v.26, n.4, p.870-878, abr. 2018. Elsevier BV. Available from: <http://dx.doi.org/10.1016/j.cjche.2017.07.015>. Acessed: Apr. 18, 2021.

YOKOYAMA, J. T.C et al. Stevia residue as new precursor of CO2-activated carbon: optimization of preparation condition and adsorption study of triclosan. **Ecotoxicology And Environmental Safety**, [S.L.], v.172, p.403-410, maio 2019. Elsevier BV. Available from: <http://dx.doi.org/10.1016/j.ecoenv.2019.01.096>. Acessed: Apr. 18, 2021.